NEOPLASIA
www.neoplasia.com

Volume 12 Number 10 October 2010 pp. 818–825 818

Longitudinal Magnetic Resonance Imaging–Based Assessment of Vascular Changes and Radiation Response in Androgen-Sensitive Prostate Carcinoma Xenografts under Androgen-Exposed and Androgen-Deprived Conditions[1]

Kathrine Røe[*,†], Therese Seierstad[*,‡], Alexandr Kristian[§], Lars Tore Gyland Mikalsen[†], Gunhild Mari Mælandsmo[§,¶], Albert J. van der Kogel[#], Anne Hansen Ree[*,†] and Dag Rune Olsen[**]

*Department of Radiation Biology, Institute for Cancer Research, The Norwegian Radium Hospital, Oslo University Hospital, Oslo, Norway; [†]University of Oslo, Oslo, Norway; [‡]Faculty of Health Sciences, Buskerud University College, Drammen, Norway; [§]Department of Tumor Biology, Institute for Cancer Research, The Norwegian Radium Hospital, Oslo University Hospital, Oslo, Norway; [¶]Department of Pharmacy, Faculty of Health Sciences, University of Tromsø, Tromsø, Norway; [#]Department of Radiation Oncology, Radboud University, Nijmegen Medical Center, Nijmegen, The Netherlands; **University of Bergen, Bergen, Norway

Abstract

Prostate cancer (PCa) patients receive androgen-deprivation therapy (ADT) to reduce tumor burden. However, complete eradication of PCa is unusual, and recurrent disease is evident within approximately 2 years in high-risk patients. Clinical evidence suggests that combining ADT with radiotherapy improves local control and disease-free survival in these patients compared with radiotherapy alone. We investigated whether vascularization of androgen-sensitive PCa xenografts changed after ADT and whether such therapy affected radiation response. CWR22 xenografts received combinations of ADT by castration (CWR22-cas) and 15 Gy of single-dose irradiation. At a shortest tumor diameter of 8 mm, vascularization was visualized by dynamic contrast-enhanced magnetic resonance imaging before radiation and 1 and 9 days after radiation. Voxel-wise quantitative modeling of contrast enhancement curves extracted the hemodynamic parameter K^{trans}, reflecting a combination of permeability, density, and blood flow. Tumor volumes and prostate-specific antigen (PSA) were monitored during the experiment. The results showed that K^{trans} of CWR22-cas tumors 36 ± 4 days after ADT was 47.1% higher than K^{trans} of CWR22 tumors ($P = .01$). CWR22-cas tumors showed no significant changes in K^{trans} after radiation, whereas K^{trans} of CWR22 tumors at day 1 decreased compared with pretreatment values ($P = .04$) before a continuous increase from day 1 to day 9 followed ($P = .01$). Total PSA in blood correlated positively to tumor volume ($r = 0.59$, $P < .01$). In conclusion, androgen-exposed xenografts demonstrated radiation-induced reductions in vascularization and tumor volumes, whereas androgen-deprived xenografts showed increased vascularization and growth inhibition, but no significant additive effect of radiation.

Neoplasia (2010) 12, 818–825

Abbreviations: ADT, androgen-deprivation therapy; DCE-MRI, dynamic contrast-enhanced magnetic resonance imaging; PCa, prostate cancer; PSA, prostate-specific antigen; ROI, region of interest; RT, radiotherapy; TE, echo time; TR, repetition time; VIF, vascular input function

Address all correspondence to: Kathrine Røe, MSc, Department of Radiation Biology, Institute for Cancer Research, Oslo University Hospital, Montebello, 0310 Oslo, Norway. E-mail: Kathrine.Roe@rr-research.no

[1]This work was financially supported by the South-Eastern Norway Regional Health Authority grant 2009070 (K.R.) and the Norwegian Cancer Society grant 80114001 (T.S.).
Received 26 March 2010; Revised 21 June 2010; Accepted 22 June 2010

DOI 10.1593/neo.10484

Introduction

Androgens are the primary regulators of prostate cancer (PCa) growth and proliferation [1]. The effects of androgen-deprivation therapy (ADT) on prostatic carcinoma are significant, particularly for clinically localized disease [2]. ADT results in a reduction of tumor cells due to a shift to quiescence and apoptosis [3,4]. Although ADT effectively causes dormancy and reduced tumor burden, complete eradication of PCa rarely occurs and biochemical progression in high-risk PCa patients receiving ADT is usually evident within 2 years. The mechanisms preceding the transition from the androgen-sensitive to the incurable androgen-resistant state of PCa are still not fully understood.

Although PCa are not considered to be highly vascular tumors, they demonstrate increased vascular endothelial growth factor expression and increased vascularization when compared with benign prostatic hyperplasia and normal prostatic tissue [1]. It has also been shown that androgens are involved in blood flow regulation *in vivo* and that androgen withdrawal affects vascular endothelial growth factor expression, microvessel density, and permeability in these tumors [1,5]. However, the vascular remodeling after ADT remains unclear and warrants further investigations. In this regard, noninvasive measurements are beneficiary to allow monitoring of changes in tumor vascularization.

Dynamic contrast-enhanced magnetic resonance imaging (DCE-MRI) allows repeated, *in vivo* visualization of tumor vasculature and is thus important in clinical response monitoring of increased or inhibited angiogenesis [6]. By applying quantitative pharmacokinetic modeling of the contrast agent uptake in tumor tissue, vascular kinetic biomarkers associated with underlying physiological processes can be derived; such markers may further be used in monitoring response to treatments and characterizing tumors [7]. One of the parameters that can be deduced from such modeling, the forward volume transfer constant between blood plasma and extravascular extracellular space, K^{trans}, has shown to reflect acute treatment-induced changes in tumor vascularization [8].

Radiotherapy (RT) is an important treatment modality for PCa, although its efficacy decreases with stage. Clinical trials have shown that the combination of neoadjuvant or adjuvant ADT with RT improves local control and disease-free survival for PCa patients compared with RT alone, especially for high-risk patients [2,9]. However, there are also evidences for the contrary, and the possibility that ADT deteriorates the tumor vascularization, thus induces increased hypoxia and reduced effect of subsequent RT, should also be considered. Technological advances of RT equipment have brought intensity-modulated RT and high–dose rate brachytherapy into the clinic, allowing increased tumor doses. These techniques rely on noninvasive imaging for accurate tumor localization; moreover, advanced imaging techniques may provide useful information about tumor biologic and physiological factors of importance to the response to therapy. In this regard, DCE-MRI represents a promising technique that has the potential of providing information about the vascularization and oxygenation in tumors and may become useful in the evaluation of RT response for PCa patients.

The specific aims of the present study were to apply DCE-MRI with subsequent pharmacokinetic analysis to investigate whether vascularization in human androgen-sensitive CWR22 PCa xenografts alters after ADT by castration and whether ADT affects radiation response.

Materials and Methods

Animals and Xenografts

Male, sexually mature BALB/c nude mice (30-35 g, 6-8 weeks old) were used in this study. The Institutional and National Committee on Research on Animal Care approved the protocol, and the experiment was performed according to Interdisciplinary Principles and Guidelines for the Use of Animals in Research, Marketing and Education (New York Academy of Science, New York, NY). The mice were bred at the animal department of our institute and kept under specific pathogen-free conditions at constant temperature (21.5-22.5°C) and humidity (50%-60%) and given sterilized food and water *ad libitum*.

Xenografts were generated by subcutaneous (s.c.) implantation of ~(2 × 2 × 2) mm^3 tumor tissue from the human androgen-sensitive CWR22 xenograft into one flank of each mouse. Procedures for implantation, growth, and harvesting of CWR22 xenografts in mice were followed according to previous reports [10,11]. Animals with CWR22 xenografts were included into the experiment when their shortest tumor diameter reached 8 mm. Androgen-deprived CWR22 xenografts, denoted CWR22-cas, were obtained by castration of animals bearing CWR22 xenografts. The surgical castration was performed at a shortest tumor diameter of 13 mm, and the animals were included into the experiment when the CWR22-cas xenografts had regressed to a shortest tumor diameter of 8 mm. The time from castration to inclusion was 36 ± 4 days. At the day of inclusion, a pretreatment (day 0) MRI was performed before each of the two groups of 16 animals (androgen-exposed and androgen-deprived) was divided into two subgroups of 8 animals: radiation and control. The tumors in the radiation groups were irradiated after the day 0 MRI. At days 1 and 9, repeated MRIs were performed on all animals in the experiment.

Thirty-two animals were randomly allocated into four groups of eight animals: CWR22 control (CWR22-C), CWR22 irradiation (CWR22-IR), CWR22-cas control (CWR22-cas-C), and CWR22-cas irradiation (CWR22-cas-IR). For the CWR22 groups, all animals were killed when the longest tumor diameter of two of the tumors in the group reached 16 mm. Animals with CWR22-cas tumors were killed 30 days after inclusion into the experiment.

To determine the mean vascular input function needed in pharmacokinetic modeling of contrast enhancement curves, eight separate tumor-bearing, male mice with identical weight and age as the other 32 animals were subjected to left cardiac ventricular DCE-MRI examinations.

In addition, six CWR22 tumors of the same size (diameter = 8 mm) were used in immunohistochemistry to assess differences in tumor vascularization, perfusion, and hypoxia between individual tumors.

Tumor Volume

Tumor volumes were estimated from caliper measurements from implantation until the end of the experiment using the formula (length × length × width) / 2, with length being the longest diameter across the tumor and width being the corresponding perpendicular diameter.

Radiotherapy

Tumors in the two radiation groups received a single dose of 15 Gy on day 0 (after preradiation MRI) using a ^{60}Co source (Mobaltron 80; TEM Instruments, Crawley, UK) with a dose rate of 0.8 Gy/min.

Anesthesia and Analgesia

Animals were anesthetized with s.c. injections of a mixture of 2.4 mg/ml tiletamine and 2.4 mg/ml zolazepam (Zoletil vet; Virbac Laboratories, Carros, France), 3.8 mg/ml xylazine (Narcoxyl vet; Roche, Basel, Switzerland), and 0.1 mg/ml butorphanol (Torbugesic; Fort Dodge Laboratories, Fort Dodge, IA), diluted 1:5 in sterile water. A dose of 50 μl/10 g of body weight was administered before radiation, and

75 μl/10 g of body weight was administered before MRI acquisitions and castration. Analgesia was provided to castrated animals by s.c. injections of buprenorphine (Temgesic; Schering-Plough, Brussels, Belgium) in a dose of 0.1 mg/kg.

DCE-MRI Acquisition

DCE-MRI of the tumors' central slice was acquired at day 0 (before radiation), day 1 (24 hours after radiation), and day 9 using a 1.5-T GE Signal LS clinical scanner (GE Medical Systems, Milwaukee, WI). Weight of individual animals determined the amount of contrast agent (Gd-DTPA; Magnevist, Schering, Berlin, Germany; diluted in heparinized saline to 0.06 M) to be administrated. Before MRI, a heparinized 24-gauge catheter attached to a cannula containing 0.01 ml/g body weight saline-diluted Gd-DTPA was inserted into the tail vein. The animals were placed in a special cradle and put into an in-house built MR mouse coil [12] before the coil was placed in the scanner. The animals' temperature was maintained at 38°C during the acquisition.

MRI included axial fast spin-echo T2-weighted images (echo time [TE_{eff}] = 85 milliseconds, repetition time [TR] = 4000 milliseconds, echo train length = 16, image matrix = 256 × 256, field of view (FOV) = 4 cm, slice thickness = 2 mm) to localize tumor, and dynamic fast spoiled gradient-recalled T1-weighted images (TE = 3.5 milliseconds, TR = 180 milliseconds, image matrix = 256 × 128, FOV = 6 cm, slice thickness = 2 mm, flip angle (FA) = 80°) to investigate contrast kinetics. After five precontrast images, Gd-DTPA was manually injected during 3 seconds before continuing dynamic postcontrast imaging for 20 minutes with 12-second time resolution. Reconstructed voxel size of T1-weighted images was 0.23 × 0.47 × 2 mm^3. Corresponding proton density images (TE = 3.5 milliseconds, TR = 360 milliseconds, image matrix = 256 × 128, FOV = 6 cm, slice thickness = 2 mm, FA = 10°) were acquired before and after DCE-MRI.

Mean vascular input functions (VIFs) were obtained from DCE-MRI of the left cardiac ventricle in eight separate male mice. The imaging protocol was identical to the one previously mentioned except for TR = 200 milliseconds for the proton density images and TR = 80 milliseconds and image matrix = 512 × 256 for the T1-weighted images (voxel size, 0.11 × 0.23 × 2 mm^3). T1-weighted imaging consisted of 120 postcontrast images acquired every 10 seconds. Cardiac gating was not used for VIF measurements; thus, to minimize motion artifacts from cardiac pulsation, mice were placed in the prone position, and phase encoding was applied in the R/L direction. The region of interest (ROI) was centered well within the left cardiac ventricle to ensure that the ROI, at all time points during the cardiac cycle, was within the cardiac ventricle.

DCE-MRI Analysis

DCE-MRI analysis was performed using in-house written programs in IDL (Interactive Data Language v6.2; Research Systems, Inc, Boulder, CO). Gd-DTPA concentrations were calculated from signal intensities and proton density images using the method of Hittmair et al. [13]. Individual VIFs were determined by fitting a biexponential function to concentration curves from the left cardiac ventricle according to VIF = $A\exp(-Bt) + C\exp(-Dt)$, with A and B representing the equilibration of Gd-DTPA between plasma and extracellular space, C and D representing kidney clearance of Gd-DTPA, and $(A + C)^{-1}$ (L/kg) representing plasma volume of the mouse per unit of body weight. A representative VIF with fitted function is shown in Figure 1. Mean VIFs for the eight mice were described by the following four parameters: A = 3.57 ± 0.34 mM, B = 0.025 ± 0.005/s, C = 1.45 ± 0.15 mM, and D = 0.0074 ± 0.0036/s. This VIF was assumed to be valid for all mice in the experiment.

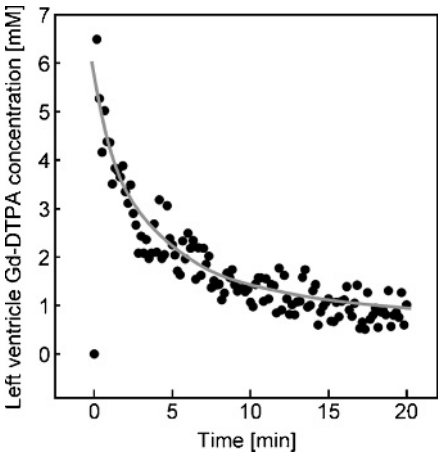

Figure 1. VIF showing left cardiac ventricle contrast enhancement as function of time after intravenous administration of Gd-DTPA. Dots represent acquired raw data and the solid line represent the fitted biexponential function.

An ROI was manually delineated around the tumor in T1-weighted images, excluding surrounding skin and connective tissue. Using the mean VIF parameters and contrast enhancement curves for individual voxels within the selected ROI, each voxel was fitted to the model of Tofts et al. [8]. Two representative contrast enhancement curves of regions with low and high contrast uptake, respectively, and the corresponding fitted Tofts functions are shown in Figure 2*A*. This allowed voxel-by-voxel estimations of the forward volume transfer

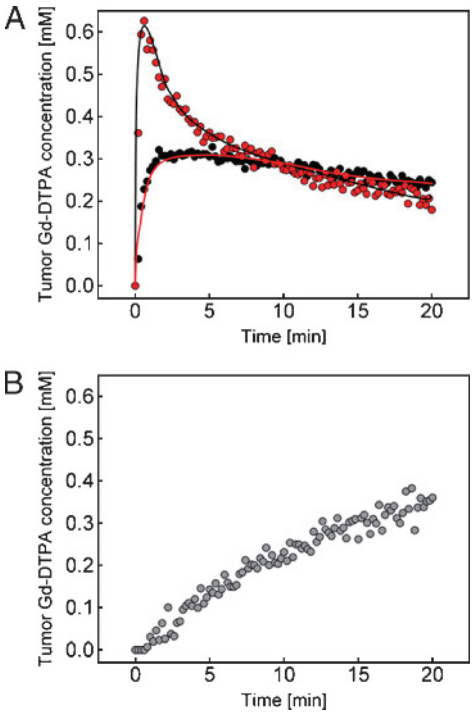

Figure 2. Representative contrast enhancement raw data curves (dots) of regions with low and high contrast uptake, respectively, with corresponding fitted Tofts functions (solid lines) (A). Example of a contrast enhancement curve in a pixel that could not be fitted to the Tofts model (B).

constant for Gd-DTPA between blood plasma and the extravascular extracellular space, K^{trans} (s^{-1}), across the tumor.

When performing Tofts modeling, not all voxels present biologically valid values of K^{trans}. For some voxels, the fit fails to converge because of low Gd-DTPA uptake or because modeling returns negative K^{trans} values. An example of a contrast enhancement curve from a voxel that cannot be fitted to the Tofts model is shown in Figure 2*B*. All these unfitted voxels were set equal to 0 and included in K^{trans} maps and in calculation of mean tumor K^{trans}. The fraction of unfitted voxels, scored as the sum of unfitted voxels *versus* the total number of voxels within the tumor ROI, was monitored to investigate the possible link between this fraction and nonviable tumor regions.

Prostate-Specific Antigen

Blood for prostate-specific antigen (PSA) analysis was collected from each animal at days 0, 1, and 9 and at the time of killing. Blood samples were allowed to coagulate before being centrifuged and frozen at −80°C until analysis. Free and total PSA were assayed using the fluoroimmunometric AutoDELFIA ProStatus PSA Free/Total kit (PerkinElmer Life and Analytical Sciences, Wallac Oy, Turku, Finland).

Immunohistochemistry

Hypoxia was determined by injecting 80 mg/kg pimonidazole hydrochloride (1-[(2-hydroxy-3-piperidinyl)propyl]-2-nitroimidazole hydrochloride; Natural Pharmaceuticals, International Inc., Research Triangle Park, NC) in 0.5 ml of saline intraperitoneally (i.p.) 60 minutes before killing the animals. Five minutes before killing the animals, 15 mg/kg Hoechst 33342 (Sigma Chemical Co, St Louis, MO) in 0.1 ml of saline was injected intravenously for determination of tumor perfusion. Immediately after dissection, tumors were frozen in liquid nitrogen and stored at −80°C until they were shipped to the Department of Radiation Oncology, Radboud University, Nijmegen Medical Center, Nijmegen, The Netherlands, for staining and imaging.

The central slice of the tumor was cut before staining and scanned according to procedures described previously [14] to obtain triple immunofluorescent images of tumor vasculature (9F1; TCL image, TNO, Delft, The Netherlands), blood perfusion (Hoechst), and hypoxia (pimonidazole).

Quantitative analysis of immunohistochemistry was performed using an in-house written program in MATLAB 7.0.1 (The MathWorks, Natick, MA). The tumor area, excluding artifacts and tissue folding, was manually identified and delineated using GIMP 2.6.4 (www.gimp.org). Pimonidazole and Hoechst stains were segmented by applying a threshold at 0.3 × 95th intensity percentile and labeled as hypoxic and perfused, respectively. The hypoxic fraction was calculated as the total number of hypoxic pixels divided by the total number of pixels in the tumor area. Vessel density was quantified as the total number of vessels, irrespective of vessel area, divided by the total tumor area. A vessel was defined as perfused if at least half of the vessel's pixels were within two pixels' rectilinear distance (5.18 μm) from a perfusion-stained pixel. Hypoxic distance histograms were calculated using the euclidean norm along the shortest straight line from each hypoxic pixel to its nearest vessel, irrespective of tumor boundaries.

Statistical Analysis

Statistical analysis was performed using SPSS 16.0 (SPSS, Cary, NC). Differences between groups and time points were analyzed using two-sided *t* tests under conditions of normality. Pearson correlation test analyzed whether correlations between variables were significant. Results are presented as mean ± SEM, and a significance level of 5% was used in all statistical analyses.

Results

Tumor Growth

Pretreatment tumor volumes were normally distributed ($P = .60$) with a mean tumor volume of 392.1 ± 37.7 mm^3. Figure 3 shows normalized tumor volumes for control and irradiated CWR22 and CWR22-cas tumors.

Exponentially growing CWR22-C tumors showed a 2.5-fold increase ($P < .01$) from day 0 to day 9. At the completion of the study, volumes of these tumors had increased 9.6-fold compared with baseline. Radiation induced an initial 0.3-fold ($P < .01$) tumor volume decrease in CWR22-IR tumors from day 0 to day 1, followed by a 1.3-fold increase in tumor volume from day 1 to day 9. CWR22-IR tumors showed growth inhibition before slowly relapsing from day 51 and onward. At day 30, mean normalized tumor volumes of CWR22-C tumors were 12-fold larger ($P < .01$) than tumor volumes of CWR22-IR tumors (Figure 3).

Volumes of tumors in the CWR22-cas cohorts decreased continuously during follow-up of the experiment. Thirty days after initiation of the study, volumes of CWR22-cas-C and CWR22-cas-IR tumors had decreased to 0.6-fold ($P < .01$) and 0.4-fold ($P < .01$) of pretreatment values, respectively.

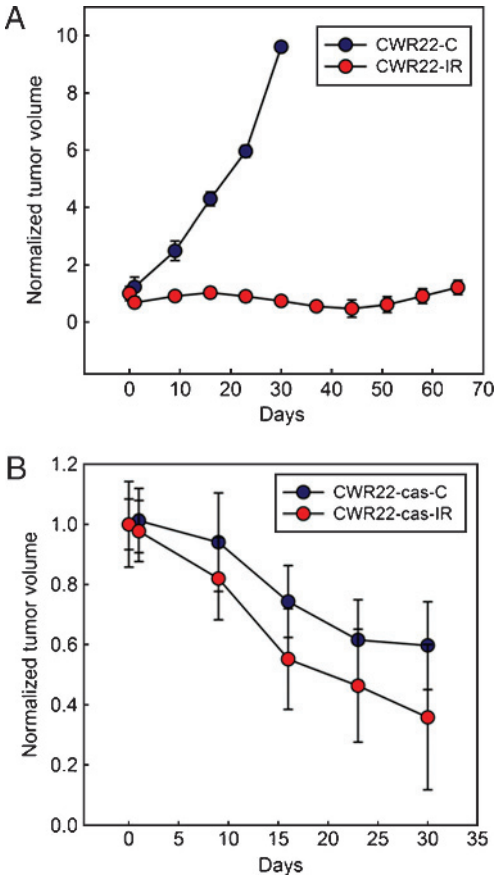

Figure 3. Tumor volumes of CWR22 (A) and CWR22-cas (B) normalized to day 0 (day of inclusion). Each time point represents normalized mean and SEM values. *C*, control tumors; *IR*, irradiated tumors receiving a single fraction of 15 Gy after the MRI at day 0.

Except for day 1, where CWR22-IR tumors showed an immediate radiation-induced reduction in tumor volume (P = .03), there were no significant differences in tumor growth between CWR22-IR tumors and androgen-deprived CWR22-cas-C tumors throughout the experiment.

Prostate-Specific Antigen

Figure 4*A* shows total PSA measured in the four groups at days 0, 1, and 9 and at the day of killing. Mean pretreatment total PSA was 30.7 ± 6.0 ng/ml for animals bearing CWR22 tumors, whereas total PSA for animals bearing CWR22-cas tumors was 18.3 ± 3.2 ng/ml. For animals bearing CWR22-C tumors, total PSA increased to 88.2 ± 12.5 ng/ml (P < .01) and 212.4 ± 13.8 ng/ml (P < .01) after 9 days and at the end of the experiment, respectively. For comparison, total PSA measured in animals with CWR22-IR tumors was 50.5 ± 10.7 ng/ml (P = .02) at day 9 and 75.8 ± 17.4 ng/ml (P = .02) at the completion of the experiment. In animals bearing CWR22-cas tumors, total PSA was reduced on all subsequent measurement days, with the decrease from day 9 to the end point being significant for both CWR22-cas-C (63.3% decrease, P < .01) and CWR22-cas-IR animals (94.3% decrease, P = .01). It was a positive correlation between total PSA and tumor volume (r = 0.59, P < .01; Figure 4*B*). The correlation was stronger for animals with CWR22 tumors (r = 0.74, P < .01) than for animals with CWR22-cas tumors (r = 0.27, P = .03). The correlation between total PSA and tumor volume was strong for both CWR22 and CWR22-cas tumors when only subjecting control tumors to analysis (r = 0.74, P < .01 and r = 0.73, P < .01, respectively).

Qualitative Assessment of DCE-MRI

An example of an anatomic T1-weighted MR image through the center of a CWR22 tumor and matched slice of K^{trans} is shown in Figure 5*A*. The black areas within the tumor ROI are unfitted voxels. Rapid contrast agent uptake was detected in the dynamic T1-weighted MR images in the peripheral regions of the tumors, whereas signal enhancement in central regions was slower. Within 20 minutes after contrast agent administration, washout of contrast agent was manifested for all tumors; however, precontrast signal intensity levels were not restored.

Treatment Monitoring Using DCE-MRI

Figure 5*B* shows pretreatment, day 1, and day 9 K^{trans} maps of a CWR22-IR tumor, whereas Figure 6 summarizes the mean tumor K^{trans} of all tumors. The mean pretreatment K^{trans} value was 47.1% higher for CWR22-cas tumors compared with CWR22 tumors (P = .01). After radiation, K^{trans} of CWR22-cas-IR tumors was unchanged when comparing with pretreatment values. Furthermore, there were no significant differences in K^{trans} between irradiated and control CWR22-cas tumors at day 1 or day 9. For CWR22-IR tumors, K^{trans} was reduced by 45.7% from day 0 to day 1 (P = .04), followed by an 87.7% increase from day 1 to day 9 (P = .01). No significant day-to-day variations were found for the CWR22-C tumors.

The decrease in K^{trans} from day 0 to day 9 for CWR22-C tumors coincided with a 38.6% increase in the fraction of unfitted voxels, giving a significant negative correlation between K^{trans} and the fraction of unfitted voxels for this group (r = –0.79, P < .01). Table 1 shows the fraction of unfitted voxels within each group at the time points for DCE-MRI.

Discussion

The present study shows that tumor vascularization is different in androgen-sensitive CWR22 xenografts under androgen-exposed and androgen-deprived conditions and that the resulting PCa phenotypes have different response to radiation.

CWR22-cas tumors had significantly higher mean K^{trans} than CWR22 tumors of the same size in noncastrated animals. Several studies have reported decreased vascularization and angiogenesis after surgical or chemical ADT. These studies have examined vascularization responses immediately or within a few days after ADT. In our study, we investigated vascularization after a longer period of androgen-deprivation (36 ± 4 days), which, when the five-times faster metabolism in mice is accounted for, corresponds to approximately 6 months in humans. This period is the same as many PCa patients receive ADT before RT treatment is initiated. Because of the controversial use of RT as an additional treatment at this time point, and also the uncertainties about the required duration of ADT before RT, we wanted to investigate this more clinically relevant time point, rather than the immediate androgen-deprivation effect. So even if volumes of CWR22-cas

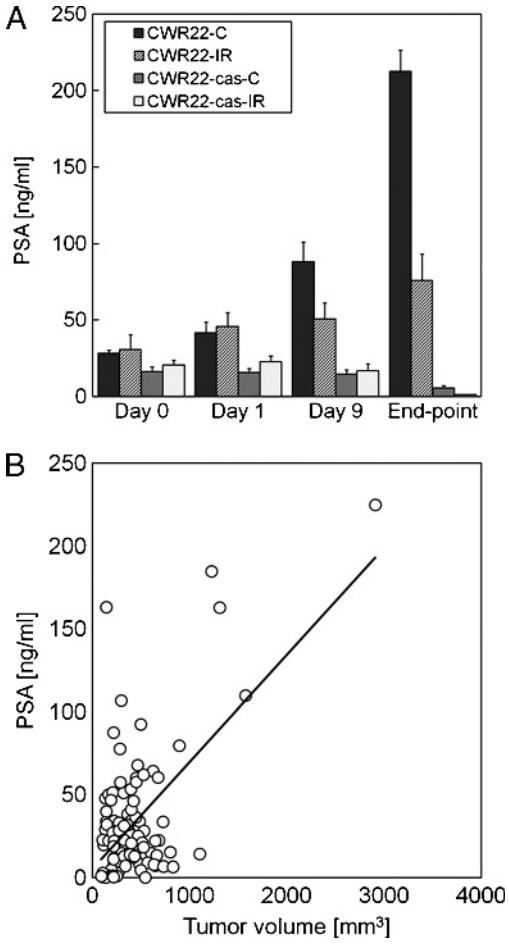

Figure 4. Total PSA in blood (mean ± SEM) at days 0, 1, and 9 and at the end of the experiment for the four treatment groups (A). *C*, control tumors; *IR*, irradiated tumors receiving a single fraction of 15 Gy after the MRI at day 0. Total PSA in blood correlated positively to tumor volume (r = 0.59, P < .01) (B). Separating CWR22 and CWR22-cas tumors, the correlation between total PSA and tumor volume was stronger for animals with CWR22 tumors (r = 0.74, P < .01) than for animals with CWR22-cas tumors (r = 0.27, P = .03).

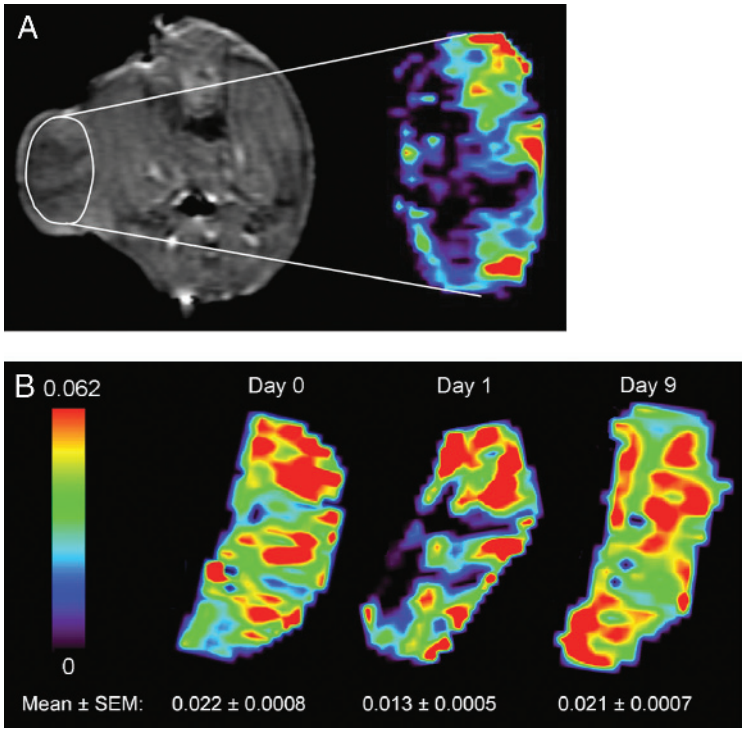

Figure 5. Anatomic T1-weighted MR image through the center of a CWR22 tumor with illustration of the delineation of tumor ROI, and the corresponding K^{trans} map within the selected ROI. The black areas within the tumor ROI are unfitted voxels (A). K^{trans} ($\times 10^{-3}$ s^{-1}) maps and mean values of a CWR22 tumor before radiation (day 0) and after radiation (days 1 and 9) (B).

tumors regressed, our MRI findings indicate an increasing tumor vascularization, when compared with exponentially growing CWR22 tumors with identical tumor volumes at the time of MRI examination.

CWR22-IR tumors showed a significant decrease in K^{trans} 1 day after receiving a single radiation dose of 15 Gy, which might result from radiation-induced reductions in blood flow, endothelial surface area, and/or vessel permeability. Together, these factors contribute to compromised inflow of contrast agent, thereby leading to slowly or nonenhancing regions in DCE-MRI and reduced tumor K^{trans}. We hypothesize that this decreased K^{trans} might be related to increased hypoxia. Because animals were imaged repeatedly (days 0, 1, and 9) and posttreatment differences in tumor growth were assessed, possible relations between K^{trans} and hypoxia were investigated in a separate experiment involving immunohistochemistry of six additional xenografts. In Figure 7, triple immunofluorescent images of tumor tissue sections from two tumors with substantially different hypoxic patterns are shown. The tumor in Figure 7*A* has an equally distributed hypoxic pattern, as opposed to the more extensive and centrally distributed hypoxic pattern surrounding blood vessels in Figure 7*B*. The hypoxic fraction was 28.1% in the left tumor and 45.3% in the right tumor, and the hypoxic distance histogram (Figure 7*C*) visualizes the differences in distances between hypoxia and vessels. The tumor with the highest

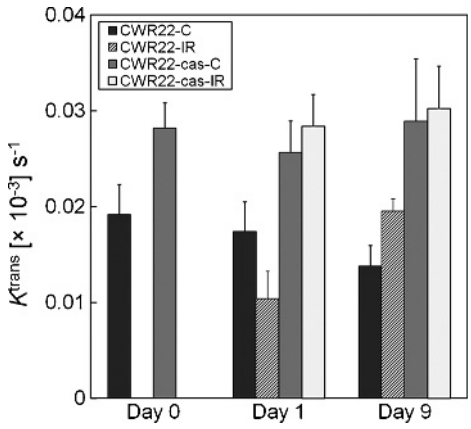

Figure 6. K^{trans} (mean ± SEM) values before radiation and 1 and 9 days after radiation. The two bars on day 0 represent pretreatment groups for 16 CWR22 tumors and 16 CWR22-cas tumors. After the day 0 MRI, each of the two groups of 16 animals was divided into two subgroups of eight animals: radiation and control. The four bars on days 1 and 9 refer to these four subgroups. *C* indicates control tumors; *IR*, irradiated tumors receiving a single fraction of 15 Gy after the MRI at day 0.

Table 1. Fraction of Unfitted Voxels from Pharmacokinetic Modeling.

	Day 0 (%)	Day 1 (%)	Day 9 (%)
CWR22			
Control	17.5 ± 6.0	14.9 ± 4.4	24.2 ± 3.2
Irradiated	12.6 ± 3.2	34.0 ± 7.2*	17.1 ± 3.2†
CWR22-cas			
Control	16.9 ± 3.3	17.5 ± 3.1	19.7 ± 2.9
Irradiated	13.4 ± 5.8	14.7 ± 6.0	25.5 ± 7.8

The fraction of unfitted voxels from pharmacokinetic modeling of DCE-MRI data for each group at the three imaging time points.

*The increase in the fraction of unfitted voxels from day 0 to day 1 in CWR22-IR tumors was significant (P = .02).

†The decrease in the fraction of unfitted voxels from day 1 to day 9 in CWR22-IR tumors was close to significant (P = .06).

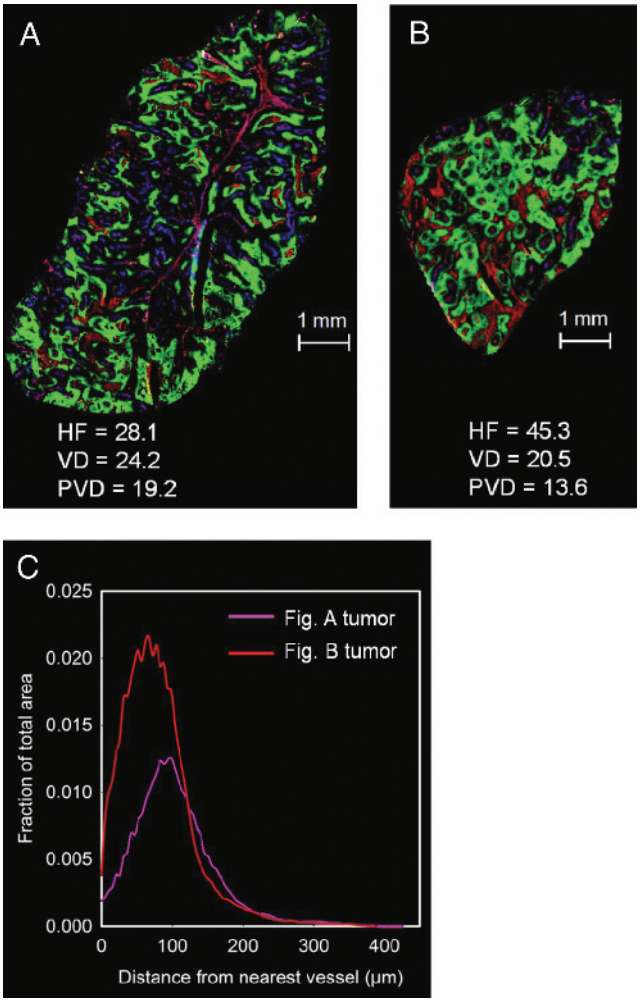

Figure 7. Triple immunofluorescent images showing vascular architecture (9F1, red), perfused vessels (Hoechst 33342, blue), and hypoxic areas (pimonidazole, green). These two images demonstrate two different hypoxia patterns: (A) hypoxia is evenly distributed across the tumor; (B) hypoxia is more extensive and is constraining the vessels. When calculating hypoxic distance diagrams (distance hypoxia − blood vessels), this distance is less in panel B than in panel A. The corresponding K^{trans} values are $0.0184 \pm 0.0004 \times 10^{-3}\ s^{-1}$ (A) and $0.0084 \pm 0.0004 \times 10^{-3}\ s^{-1}$ (B). *HF* indicates hypoxic fraction (%); *PVD*, perfused vessel density (vessels/mm^2); *VD*, vessel density (vessels/mm^2).

hypoxic fraction, where hypoxia confined the vessels, demonstrated a lower K^{trans} value ($0.0084 \pm 0.0004 \times 10^{-3}\ s^{-1}$) than the less hypoxic tumor ($0.0184 \pm 0.0004 \times 10^{-3}\ s^{-1}$). These two images illustrate that the appearance and amount of hypoxia might be the cause of altered K^{trans} values. In addition, the presence of hypoxia is a well-known factor of significant importance in PCa, by promoting tumor progression and impairing treatment responses [15].

In contrast to the poorly vascularized androgen-exposed CWR22 tumors, irradiation of the well-vascularized androgen-deprived CWR22-cas tumors did not significantly alter the K^{trans} values. Whereas oxygen consumption depends on the cells' respiratory activity and cell density, the oxygen supply is primarily determined by blood perfusion and microvascular density [16]. Thus, the high K^{trans} values of the androgen-deprived tumors are anticipated to be related to increased tumor oxygenation, which is a beneficiary condition in RT response. An open phase 3 study recently showed that patients with androgen-sensitive PCa receiving 3 months of ADT before combined ADT and RT halved the PCa-specific mortality and decreased the risk of PSA relapse relative to those receiving ADT alone [2].

In our study, radiation did not represent an additive effect on growth inhibition of androgen-deprived CWR22-cas tumors. The dominating effect of ADT alone on growth inhibition might have marginalized the contribution of radiation to the overall effect. Moreover, killing the animals in the androgen-deprived groups 30 days after initiation of ADT could have been too early, thereby missing the opportunity to resolve an enhanced effect of the combination of ADT and RT over RT only.

The unfitted voxels from the pharmacokinetic modeling of contrast uptake in tumor tissue were set to 0 and included in the calculation of mean tumor K^{trans}. It has previously been shown that the fraction of unfitted voxels is strongly correlated to tumor necrosis, and consistent with this, exclusion of fit failures from mean tumor K^{trans} calculation eliminates this correlation [17]. Thus, by excluding unfitted voxels, K^{trans} is essentially determined from the viable tumor tissue, excluding necrotic hypoperfused regions. Bradley et al. [17] and Galbraith et al. [18] proposed that these posttherapy low-enhanced voxels can be a useful noninvasive biomarker of tumor necrosis, providing support for including these voxels in our K^{trans} calculations. The largest increase in the fraction of unfitted voxels was found in the tumors responding to treatment (CWR22-IR), reflected by reduced tumor K^{trans} and reduced tumor volumes. Thus, we hypothesize that necrosis might the major factor determining this fraction. However, because we performed longitudinal MRI of all tumors, tumor histology with quantification of necrosis could not be obtained simultaneously, and thus, the validity of this hypothesis requires further investigations in a separate study.

The model of Tofts and Kermode assumes the contrast agent to be instantly mixed in the plasma. In our experimental study, this assumption is reasonable as the blood circulation time in mice is short relative to the injection time. The use of K^{trans} as a measure of vascularization also assumes that blood flow is not flow limited and that flow is always greater than permeability [8]. Thus, especially for large tumors with necrotic cores or irradiated tumors, precaution should be taken when analyzing and interpreting results. However, much of the low-flow areas in the center of the tumors were unfittable, and thus, this is taken into account by including these voxels in the mean tumor K^{trans} calculations.

We found that total PSA in CWR22 xenografts was positively correlated to tumor volumes. Furthermore, blood levels of PSA were decreasing after ADT. This is in accordance with findings from other groups using CWR22 xenografts in preclinical studies [10,19]. The use of functional imaging technologies, such as positron emission tomography (PET) and MRI, has revealed that changes in tumor biology and physiology precede changes in PSA. The rapid postradiation decrease of K^{trans} in our CWR22 tumors did not coincide with decreased PSA values, suggesting the possibility of using K^{trans} as an early predictor of treatment response. Rather than showing reduced PSA values, the CWR22 tumors demonstrated a slow increase after radiation. This has also been shown by others [19] and can be explained by the low time resolution of PSA measurements with the possibility of missing an eventual transient decrease in PSA. However, the increase in K^{trans} of CWR22 tumors at day 9 coincides with the increased PSA.

The CWR22 xenograft is derived from a patient's primary tumor being androgen-sensitive [10,11,20], providing a valuable model of the

clinical situation of localized PCa, because this xenograft model regresses after ADT and shows stability before recurring growth in the androgen-resistant state is evident. Although the androgen-deprivation response characteristics of CWR22 xenografts seem to be representative of many PCa, the heterogeneous clinical responses of human tumors should be considered when making extrapolations. Notwithstanding, the parallels between the CWR22 xenograft model and many human PCa suggest that inferences based on the presented results apply to a significant proportion of human PCa.

To summarize, we here present the radiation response of both androgen-exposed and androgen-deprived CWR22 xenografts. Further, we use *in vivo* DCE-MRI as a method, with the hemodynamic transfer constant K^{trans} as a biomarker, to noninvasively and repeatedly assess tumor vascularization in these two phenotypes. The study detected radiation-induced reductions of K^{trans} values and tumor volumes in androgen-exposed xenografts, whereas ADT induced substantially increased K^{trans} values along with growth inhibition. No significant additive effect of radiation was, however, seen in the androgen-deprived xenografts. The presented results have encouraged future expansion of the current study into more advanced stages of PCa after ADT, also incorporating investigations of the role of hypoxia in the transition from androgen-sensitive to androgen-resistant disease.

Acknowledgments

The authors thank E. Paus and coworkers at the Central Laboratory, Department of Medical Biochemistry, Oslo University Hospital, for excellent technical assistance with PSA analysis and F. Saatcioglu at the Department of Molecular Biosciences, University of Oslo, for providing the CWR22 xenograft model.

References

[1] Nicholson B and Theodorescu D (2004). Angiogenesis and prostate cancer tumor growth. *J Cell Biochem* **91**(1), 125–150.

[2] Widmark A, Klepp O, Solberg A, Damber JE, Angelsen A, Fransson P, Lund JA, Tasdemir I, Hoyer M, Wiklund F, et al. (2009). Endocrine treatment, with or without radiotherapy, in locally advanced prostate cancer (SPCG-7/SFUO-3): an open randomised phase III trial. *Lancet* **373**(9660), 301–308.

[3] Westin P, Stattin P, Damber JE, and Bergh A (1995). Castration therapy rapidly induces apoptosis in a minority and decreases cell proliferation in a majority of human prostatic tumors. *Am J Pathol* **146**(6), 1368–1375.

[4] Pollack A, Joon DL, Wu CS, Sikes C, Hasegawa M, Terry NH, White RA, Zagars GK, and Meistrich ML (1997). Quiescence in R3327-G rat prostate tumors after androgen ablation. *Cancer Res* **57**(12), 2493–2500.

[5] Jain RK, Safabakhsh N, Sckell A, Chen Y, Jiang P, Benjamin L, Yuan F, and Keshet E (1998). Endothelial cell death, angiogenesis, and microvascular function after castration in an androgen-dependent tumor: role of vascular endothelial growth factor. *Proc Natl Acad Sci USA* **95**(18), 10820–10825.

[6] Hillman GG, Singh-Gupta V, Zhang H, Al-Bashir AK, Katkuri Y, Li M, Yunker CK, Patel AD, Abrams J, and Haacke EM (2009). Dynamic contrast-enhanced magnetic resonance imaging of vascular changes induced by sunitinib in papillary renal cell carcinoma xenograft tumors. *Neoplasia* **11**(9), 910–920.

[7] Cho HJ, Ackerstaff E, Carlin S, Lupu ME, Wang Y, Rizwan A, O'Donoghue J, Ling CC, Humm JL, Zanzonico PB, et al. (2009). Noninvasive multimodality imaging of the tumor microenvironment: registered dynamic magnetic resonance imaging and positron emission tomography studies of a preclinical tumor model of tumor hypoxia. *Neoplasia* **11**(3), 247–259.

[8] Tofts PS, Brix G, Buckley DL, Evelhoch JL, Henderson E, Knopp MV, Larsson HB, Lee TY, Mayr NA, Parker GJ, et al. (1999). Estimating kinetic parameters from dynamic contrast-enhanced T(1)-weighted MRI of a diffusable tracer: standardized quantities and symbols. *J Magn Reson Imaging* **10**(3), 223–232.

[9] Lee AK (2006). Radiation therapy combined with hormone therapy for prostate cancer. *Semin Radiat Oncol* **16**(1), 20–28.

[10] Wainstein MA, He F, Robinson D, Kung HJ, Schwartz S, Giaconia JM, Edgehouse NL, Pretlow TP, Bodner DR, and Kursh ED (1994). CWR22: androgen-dependent xenograft model derived from a primary human prostatic carcinoma. *Cancer Res* **54**(23), 6049–6052.

[11] Nagabhushan M, Miller CM, Pretlow TP, Giaconia JM, Edgehouse NL, Schwartz S, Kung HJ, de Vere White RW, Gumerlock PH, Resnick MI, et al. (1996). CWR22: the first human prostate cancer xenograft with strongly androgen-dependent and relapsed strains both *in vivo* and in soft agar. *Cancer Res* **56**(13), 3042–3046.

[12] Seierstad T, Roe K, and Hovik B (2007). Construction of a modified capacitive overlap MR coil for imaging of small animals and objects in a clinical whole-body scanner. *Phys Med Biol* **52**(22), N513–N522.

[13] Hittmair K, Gomiscek G, Langenberger K, Recht M, Imhof H, and Kramer J (1994). Method for the quantitative assessment of contrast agent uptake in dynamic contrast-enhanced MRI. *Magn Reson Med* **31**(5), 567–571.

[14] Schuuring J, Bussink J, Bernsen HJ, Peeters W, and van der Kogel AJ (2006). Effect of carbogen breathing on the radiation response of a human glioblastoma xenograft: analysis of hypoxia and vascular parameters of regrowing tumors. *Strahlenther Onkol* **182**(7), 408–414.

[15] Marignol L, Coffey M, Lawler M, and Hollywood D (2008). Hypoxia in prostate cancer: a powerful shield against tumour destruction? *Cancer Treat Rev* **34**(4), 313–327.

[16] Hockel M and Vaupel P (2001). Tumor hypoxia: definitions and current clinical, biologic, and molecular aspects. *J Natl Cancer Inst* **93**(4), 266–276.

[17] Bradley DP, Tessier JJ, Ashton SE, Waterton JC, Wilson Z, Worthington PL, and Ryan AJ (2007). Correlation of MRI biomarkers with tumor necrosis in Hras5 tumor xenograft in athymic rats. *Neoplasia* **9**(5), 382–391.

[18] Galbraith SM, Maxwell RJ, Lodge MA, Tozer GM, Wilson J, Taylor NJ, Stirling JJ, Sena L, Padhani AR, and Rustin GJ (2003). Combretastatin A4 phosphate has tumor antivascular activity in rat and man as demonstrated by dynamic magnetic resonance imaging. *J Clin Oncol* **21**(15), 2831–2842.

[19] Dyke JP, Zakian KL, Spees WM, Matei C, Chen Y, Mao X, Shungu DC, and Koutcher JA (2003). Metabolic response of the CWR22 prostate tumor xenograft after 20 Gy of radiation studied by ^{1}H spectroscopic imaging. *Clin Cancer Res* **9**(12), 4529–4536.

[20] Pretlow TG, Wolman SR, Micale MA, Pelley RJ, Kursh ED, Resnick MI, Bodner DR, Jacobberger JW, Delmoro CM, and Giaconia JM (1993). Xenografts of primary human prostatic carcinoma. *J Natl Cancer Inst* **85**(5), 394–398.